JOURNAL OF GEOPHYSICAL RESEARCH, VOL. 104, NO. C9, PAGES 21,021–21,032, SEPTEMBER 15, 1999

Sea surface temperature variability off southern Brazil and Uruguay as revealed from historical data since 1854

Peter O. Zavialov[1]

Department of Physics, University of Rio Grande, Rio Grande, Brazil

Ilana Wainer

Oceanographic Institute, University of São Paulo, São Paulo

João M. Absy

Department of Physics, University of Rio Grande, Rio Grande, Brazil

Abstract. About 300,000 quality-controlled local reports from ships of opportunity were complemented with the data extracted from global data records to compile monthly series of sea surface temperature (SST) for the period 1854 to 1994 on a grid 1° × 1° in latitude and longitude. These historical data are used to investigate the variability off the coast of southern Brazil and Uruguay in a broad range of temporal scales from seasonal to secular. With respect to behavior at these scales, three distinct areas can be identified in the study region. The first one, located over the shelf and controlled by winter invasions of subantarctic water along with Rio de la Plata and Patos-Mirim discharges, is characterized by large annual range of SST (7° to over 10°C), energetic mean square variability (from 1.4 to 2.2°C^2, after removal of seasonal signal), and an extremely high secular trend toward warming (1.2 to 1.6°C per 100 years), especially in the proximity of the estuaries. The second one, an area of the Brazil Current influence, exhibits smaller annual range (5° to 7°C) and mean square variability (1 to 1.4°C^2). The secular trend is from 1° to 1.2°C per 100 years, smaller than observed in the shelf, but still high compared to the global average. The third area, which encompasses the eastern deep ocean part of the region away from the influence of either major currents or coastal discharges, exhibits less energetic variability at all examined scales, as compared to the rest of the region. Everywhere in the region, 50 to 80% of interannual variability is associated with periods smaller than 10 years; however, compared to the rest of the region, the shelf zone is characterized by a relatively large contribution from decadal and interdecadal scales. In austral winter a thermal front forms in the study region, separating warm tropical water associated with the Brazil Current and cold subantarctic water flowing northward on the shelf with an admixture of coastal freshwater discharges. The position of this frontal zone is subject to strong year-to-year changes. More than a half of the energy of these migrations resides at periods smaller than 10 years where the spectrum is fairly white. In the interdecadal part of the spectrum, at least three significant individual peaks can be identified, corresponding to periods of 47 ± 2, 27 ± 1, and 18 years.

1. Introduction

The region of this study (Figure 1) lies between 27° and 35° of southern latitude and between 41° and 54° of western longitude, in the northern vicinity of the mean position of the Brazil-Malvinas confluence, which is a frontal zone formed by the encounter between the southward flowing, warm, and salty Brazil Current and cold, relatively fresh Malvinas Current flowing north [e.g., *Gordon*, 1981]. The confluence region, one of the most energetic areas of the world ocean [*Chelton et al*., 1990], is characterized by strong thermohaline gradients and intense mesoscale activity [e.g., *Gordon*, 1989; *Cheney et al*., 1983]. The confluence presents large meridional migrations at both seasonal and interannual scales, moving from 40°–46°S in austral summer [e.g., *Legeckis and Gordon*, 1982] to as far north as 35–30°S in austral winter [e.g., *Ciotti et al*., 1995].

The shelf circulations in the region show intrinsic properties related, in particular, to major freshwater inputs from the Rio de la Plata and the Patos-Mirim lagoon complex [e.g., *Hubold*, 1980; *Ciotti et al*., 1995]. Coastal waters discharged from the estuaries tend to propagate northward over the shelf [*Zavialov et al*., 1998]. In austral winter a thermal front forms in the study region, separating warm tropical water associated with the Brazil Current and cold subantarctic water flowing northward on the shelf with an admixture of coastal freshwater discharges. In summer, shelf break upwelling occurrences have been registered along the coast [*Podesta*, 1990].

The behavior of the confluence region at different temporal scales and interactive relationship of this behavior with climate variability have been a subject of growing interest and exten-

[1]Now at Laboratory of Experimental Physics of the Ocean, P. P. Shirshov Institute of Oceanology, Moscow.

Paper number 1998JC900096.
0148-0227/99/1998JC900096$09.00

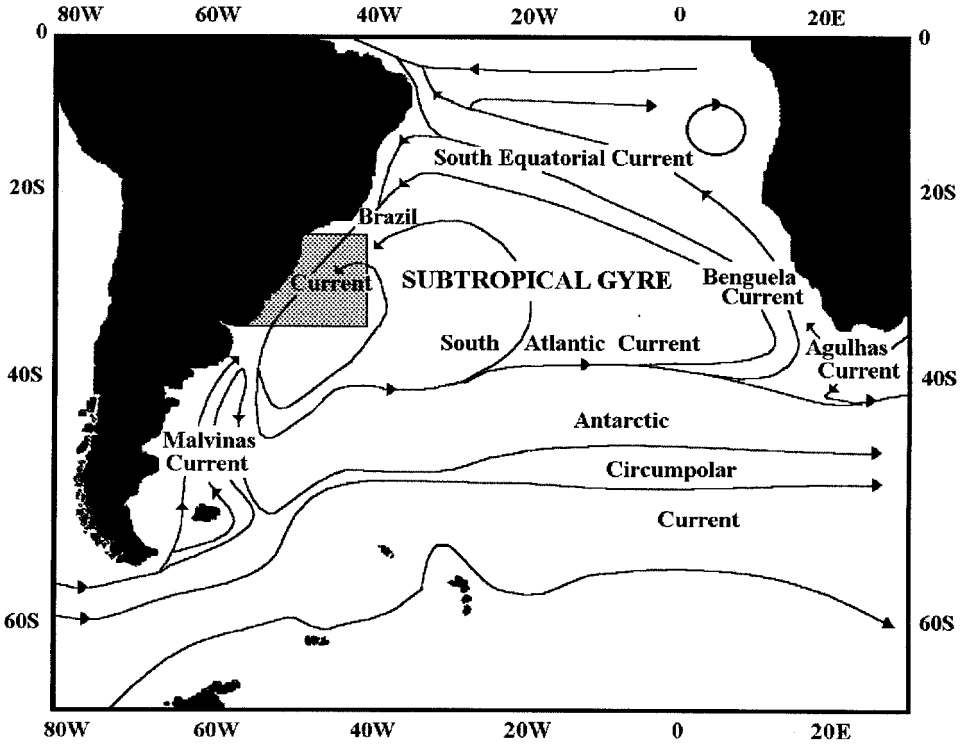

Figure 1. Scheme of general upper level circulation in South Atlantic (redrafted from *Peterson and Stramma* [1991]). The gray shading indicates the region of this study.

sive studies [e.g., *Gordon*, 1981; *Gordon and Greengrove*, 1986; *Roden*, 1986; *Reid*, 1989; *Garzoli and Garaffo*, 1989; *Olson et al*., 1988; *Gordon*, 1989; *Confluence Principal Investigators*, 1990; *Garzoli and Simonato*, 1990; *Maamaatuaiahutapu et al*., 1992; *Provost et al*., 1992; *Garzoli*, 1993; *Matano et al*., 1993; *Garzoli and Giulivi*, 1994]. However, most previous works have addressed annual or shorter temporal scales. The interannual and, especially, decadal and interdecadal variability in the region is less well known. Besides, most previous research was focused on the deep ocean part of the area while the variability over the continental shelf, which is fairly wide in the region, has been investigated to a lesser extent.

In the present study we use a blended set of historical data (1854–1994) and investigate sea surface temperature (SST) variability in a broad range of temporal scales from seasonal to secular. We seek to answer the following three general questions: (1) What are the magnitude and characteristic temporal scales of interannual to interdecadal SST variability, and how is this variability spatially distributed within the region of our interest? (2) How large is the secular trend of SST in the region, and how is it spatially distributed? (3) How large are the interannual changes in the position of the winter frontal zone on the shelf, and what are the characteristic temporal scales (i.e., spectral content) of these migrations?

The synthesized historical data set used in this study and the data analysis procedure are described in section 2. The results are presented in section 3. Subsection 3.1 addresses seasonal variability of SST, which, although not among the primary targets of this study as stated above, was investigated first in order to subtract the seasonal signal from the data. Results on the secular trends of SST are presented in subsection 3.2. In subsection 3.3 we discuss interannual to interdecadal variability of SST. Finally, in subsection 3.4 we try to assess the low-frequency variability of the frontal zone position. Discussion and conclusions are presented in section 4.

2. Data and Procedure

Since the focus of this work is on low-frequency variability in a highly energetic oceanic region, our first goal was to obtain the longest available time series of observed SST, while maintaining the highest possible spatial resolution, in this case, $1° \times 1°$. In some areas of the ocean, historical data may locally provide significantly better coverage than that feasible at a global scale. This is probably the case for the region of our interest, which has been characterized by intense commercial and fishery navigation over the last 2 centuries.

A core of the data set used in this study was made up of over 300,000 individual surface marine observations collected between 1854 and 1979, mostly by ships of opportunity and accumulated by the U.S. National Climatic Center (tape data family 11). The historical data corresponding to the region of our interest were extracted and quality controlled by *Bakun and Parrish* [1990, 1991]. This regional data set was also used previously by *Lima and Castello* [1995] and *Lima et al*. [1996]. The original reports contained the data on SST, air temperature, and wind speed. The present study is confined to analysis of SST data (the air temperature variability derived from the data set is addressed by *Absy and Zavialov* [1999]). Individual maritime reports were grouped by 1° latitude/longitude areal quadrangles and by 1-month segments of the calendar year. In this way we compiled monthly series of SST averages from 1854 to 1979, on a regular rectangular grid $1° \times 1°$ in latitude and longitude. Month/grid nodes that had less than five individual reports were considered to have insufficient data and were left blank.

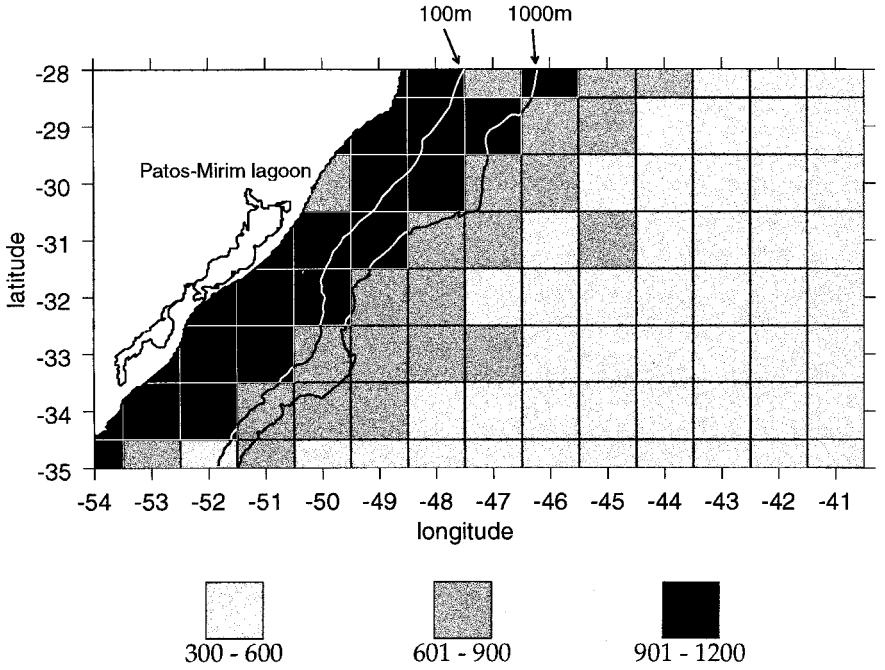

Figure 2. The study region. Indicated with gray scale in the mosaic is spatial coverage of the data measured as a number of individual months that have data at a given grid node. Contours show 100- and 1000-m isobaths.

The local historical data, available only until 1979, were then complemented with the monthly "optimum interpolation" (OI) SSTs for 1981–1994 [e.g., *Reynolds and Smith*, 1994]. These OI fields were produced based on the U.S. National Meteorological Center (NMC) file of in situ surface marine observations, blended with satellite-based SSTs, which served to improve the analysis in the areas with inadequate in situ sampling. The satellite retrievals have undergone an extensive procedure of correction for biases relative to the in situ data and were "tuned" by regression against quality-controlled surface observations as described in detail by *Reynolds* [1988], *Reynolds et al*. [1989], *Reynolds and Marisco* [1993], and *Reynolds and Smith* [1994].

Thus, by combining the sources described above and extracting the data corresponding to the region of interest, we assembled a regional set of historical SST data covering the 141-year-long period from 1854 to 1994, with temporal resolution of 1 month, albeit with a number of gaps, especially in the beginning of the series. The SST series were constructed at 88 nodes of $1° \times 1°$ grid (the remaining 38 elements of the grid correspond to land). Details and preliminary analysis of the synthesized data set were previously reported by *Zavialov and Kim* [1996], *Kim and Zavialov* [1996], and *Zavialov and Absy* [1997]. The maximum possible number of individual months filled with data at each of the grid nodes is 1692 (i.e., 12 months $\times$ 141 years). However, because of the gaps in the data, the actual number of data in the series varied between 300 and 1200. The overall data coverage, which is quite good over the shelf but decreases offshore, is shown as a mosaic in Figure 2 along with bathymetry contours. Two examples of 88 SST series used in the study are given in Figure 3 (the series are plotted only for the last 90 years, because the earlier data are too scarce to draw a continuous curve at monthly resolution).

Having obtained the time series, we computed the mean seasonal cycle of SST at all grid nodes. The properties of seasonal variability inferred thereby will be discussed in subsection 3.1. Then, we subtracted the overall means for each respective month from the original time series. This procedure served to explicitly remove the mean SST and the seasonal cycle and thus left us with 88 series of SST anomalies. The secular trend was then found at all grid nodes as a best linear fit to a corresponding series of anomalies (subsection 3.2). We then subtracted the trend from the anomalies series and computed the mean square variability, whose spatial pattern and spectral content are discussed in subsection 3.3.

An important part of this work is the investigation of interannual migrations of the frontal zone on the shelf. This front appears in the region of interest only in austral winter. We will confine this part of discussion to the month of July, which had the best historical data coverage of all winter months. As an indicator of the position of the front, we adopted the 17°C isotherm of SST. This is illustrated by Figure 4, which shows mean SST fields for the months of January and July. While in summer, temperature distribution is predominantly zonal, in winter a thermal front, oriented at an acute angle relative to the coast, forms on the shelf. The front, which in individual years is typically much sharper than it appears in overall average in Figure 4b, separates relatively warm (SSTs above 17°C) waters associated with the Brazil Current from shelf waters as cold as 13° to 16°C. Therefore the 17°C isotherm (as highlighted in Figure 4), though not necessarily coincident with the front, lies very close to it [see also *Lima and Castello*, 1995]. On the basis of the synthesized historical data, we constructed a set of maps showing the July position of the 17°C SST isotherm for 104 individual years (the remaining 37 years did not have sufficient data for the month of July). The isotherm position exhibits remarkable interannual variability. In order to quantitatively assess the interannual variability of the front position, we parameterized it by a single number, i.e., the northernmost

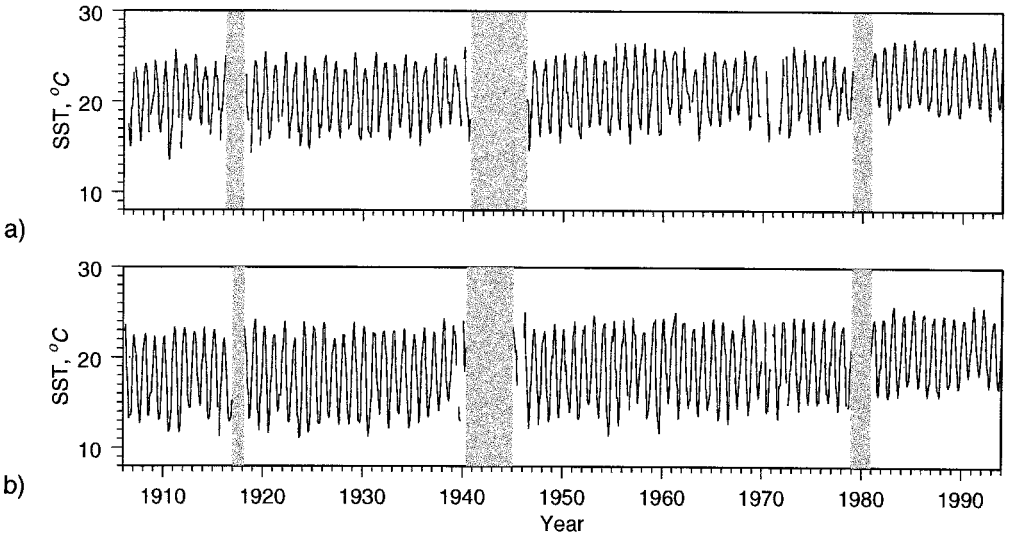

Figure 3. Examples of raw sea surface temperature (SST) series, corresponding to the grid nodes at (a) 28°S, 48°W and (b) 32°S, 51°W. The series are plotted only for the last 90 years, because the earlier data are too scarce to draw a continuous curve at monthly resolution. Shaded are principal gaps in the data.

latitude of the 17°C isotherm (typically, this is the latitude at which the isotherm merges into the coast). We then performed spectral analysis on the series of this northernmost latitude (subsection 3.4).

Conventional methods of computing power spectra, such as fast Fourier transform (FFT), require that the input data be evenly spaced in time, which is not the case in this study because of the gaps in the data. For this reason and following [*Provost et al*., 1992], the spectra were computed using an alternative technique of the so-called Lomb-Scargle periodograms [*Lomb*, 1976; *Scargle*, 1982; *Horne and Baliunas*, 1986]. The normalized spectral power as a function of angular frequency ω was computed as

$$P(\omega) = \frac{1}{2\sigma^2}\left(\frac{\left[\sum_j (T_j - T) \cos \omega(t_j - \tau) \right]^2}{\sum_j \cos^2 \omega(t_j - \tau)} + \frac{\left[\sum_j (T_j - T) \sin \omega(t_j - \tau) \right]^2}{\sum_j \sin^2 \omega(t_j - \tau)} \right) \quad (1)$$

where T_j $(j = 1, \ldots, N)$ are data values corresponding to moments of time t_j; T and σ are the overall mean and root-mean-square variance, respectively; and τ is such that

$$\tan(2\omega\tau) = \sum_j \sin(2\omega t_j) \Big/ \sum_j \cos(2\omega t_j)$$

This procedure is, of course, essentially equivalent to Fourier transform but technically free of the evenly spaced data requirement. Another advantage of this method is that it allows a simple way to compute significances and uncertainty of spectral peaks. The corresponding formulas and other details are given by *Provost et al*. [1992].

3. Results

3.1. Seasonal Variability

The mean seasonal cycle of SST was computed at all grid nodes. That is, we obtained 88 sequences of 12 SST values, each value found as an average over 141 years for a given month of the calendar year. Further, we computed the range of this seasonal cycle, found simply as the difference between the maximum and the minimum of the 12 monthly SST values. The spatial distribution of the seasonal range, which varies from less than 5°C to over 10°C, can be seen in Figure 5a. It is interesting to investigate how much of this seasonal variability is due to dynamical mechanisms, such as advection, compared to insolation. For this purpose, we prepared a map of the seasonal range with its zonal average removed (Figure 5b). Since solar irradiance depends mostly on latitude, the subtraction of zonal average should eliminate the effect of insolation, leaving us therefore only with the part of seasonal variability related to dynamical factors.

Figure 6 represents the residual between the seasonal cycle and the single annual frequency sinusoidal inference. The latter was found at all grid nodes as the best sinusoidal fit ("Bayesian inference," following the terminology of *Provost et al*. [1992]) to the observed seasonal cycle. The residual in Figure 6 is expressed as percent, relative to the total seasonal range. The magnitude of the residual characterizes essentially the departure of seasonal cycle from the ideal sinusoidal shape of annual harmonic.

3.1.1. Deep ocean part of the region. In the offshore part of the region the seasonal range is between 5°C and 6°C (Figure 5a; see also Figure 4) and its distribution is fairly uniform. The seasonal variability in this area is almost fully controlled by solar irradiance (as it follows from Figure 5b, the contribution of other mechanisms in the annual range is no larger than 1°C). Perhaps for this reason, the seasonal cycle in the southeastern part of the region is very close to a single-frequency sinusoidal

curve. As can be seen in Figure 6, the residual after removal of annual harmonic is a mere 5 to 10%. However, in the northern and central parts of the region, a tongue-like pattern with relatively high values (up to 25%) of the residual can be seen, which is likely to be related to the Brazil Current flowing south along the continental slope. The advective transport of Brazil Current is a subject of seasonal modulation itself [e.g., *Olson et al*., 1988; *Matano*, 1993; *Matano et al*., 1993], not necessarily coincident in phase with the insolation. In consequence, this may lead to the departure of SST from an ideal sinusoidal seasonal cycle.

3.1.2. Continental shelf. The seasonal range on the shelf is larger than that in the deep ocean part of the region and increases toward the shore. Near the coast in the southwestern part of the region, it is as large as 10°C. These figures are in good agreement with the findings of *Provost et al*. [1992], who investigated seasonal cycle in the adjacent area south of 35°S. On the shelf the seasonal range isopleths are organized in a tongue-like pattern, narrowing northward. This shape suggests that the larger amplitudes observed adjacent to the coast may be related to the intrusions of subantarctic water, which are typical for winter, with the addition of coastal waters originated from the Rio de la Plata and Patos-Mirim estuaries. As illustrated in Figure 5b, the dynamical factors are important and add up to 4°C to the seasonal range of SST on the southern shelf. It is interesting to observe that the zero contour in Figure 5b, corresponding to null influence from dynamical mechanisms, almost coincides with the shelf break, which is virtually the line of "no motion" separating the Brazil Current flowing south along the continental slope and the northward flow on the shelf.

The residual after the removal of annual harmonic is high on the shelf and accounts for up to 35% of seasonal range (Figure 6), which may be attributed to the dynamical influence of subantarctic and shelf waters from the south. The semiannual and higher harmonics are important in temporal behavior of the Rio de la Plata inflow [e.g., *Provost et al*., 1996, *Guerrero et al*., 1997]. Both the invasions of subantarctic water in winter and the assimilation of river discharges should favor large SST residuals from an ideal annual cycle.

In both the oceanic and the shelf parts of the study area, the

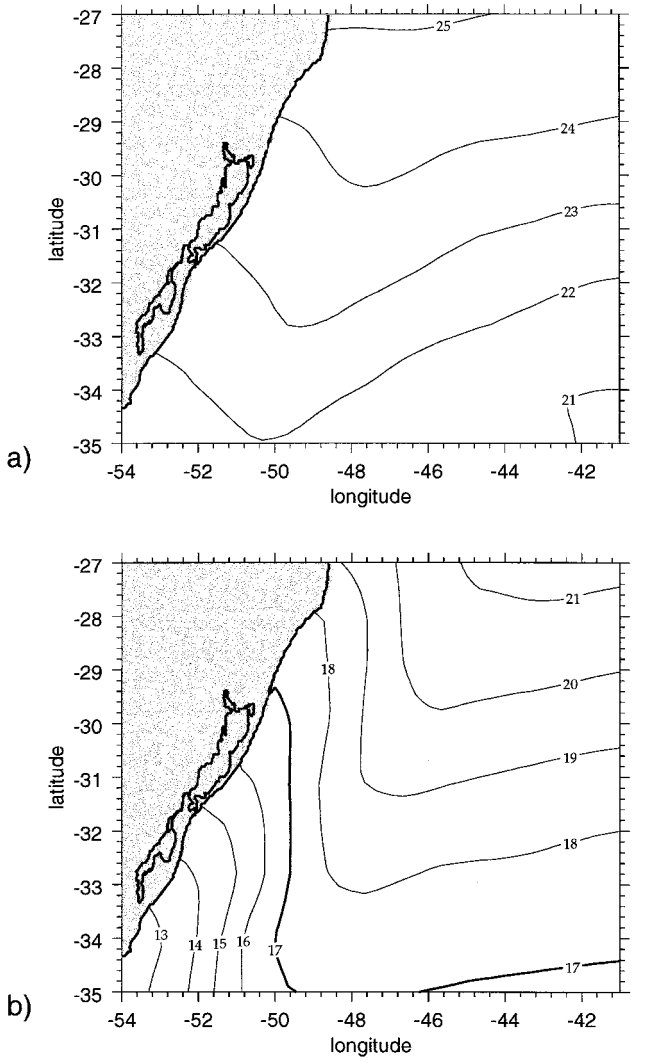

Figure 4. Overall mean SST fields for (a) January and (b) July. The 17°C isotherm, used in this study as an indicator of frontal zone in winter, is shown in bold in Figure 4b.

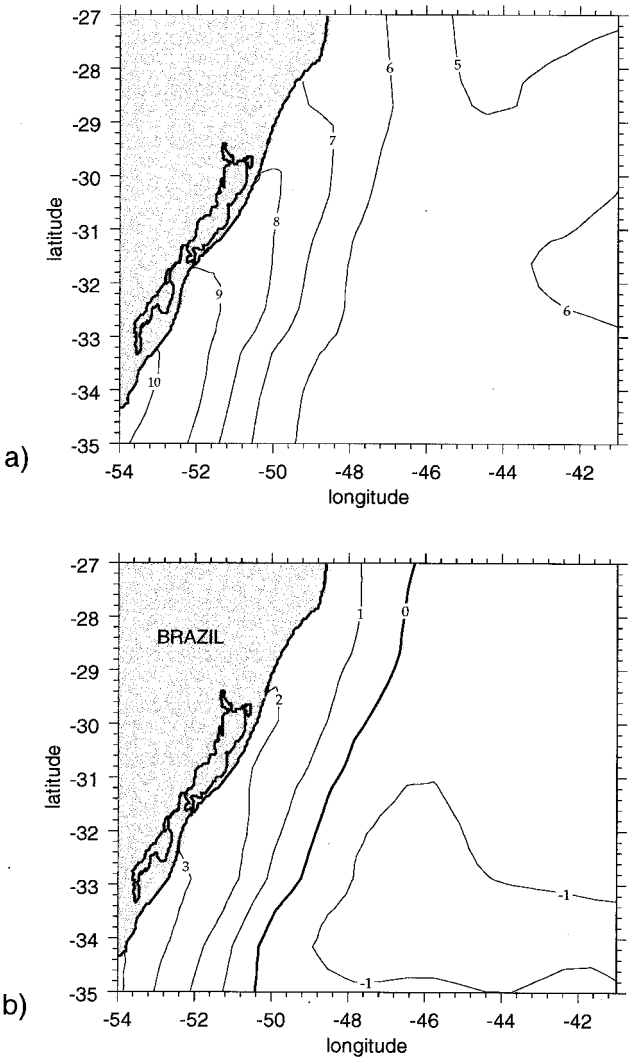

Figure 5. (a) Annual range of SST, in degrees Celsius, and (b) after removal of the zonal average in order to isolate the part of the seasonal variability attributed to dynamical effects (see text for explanation).

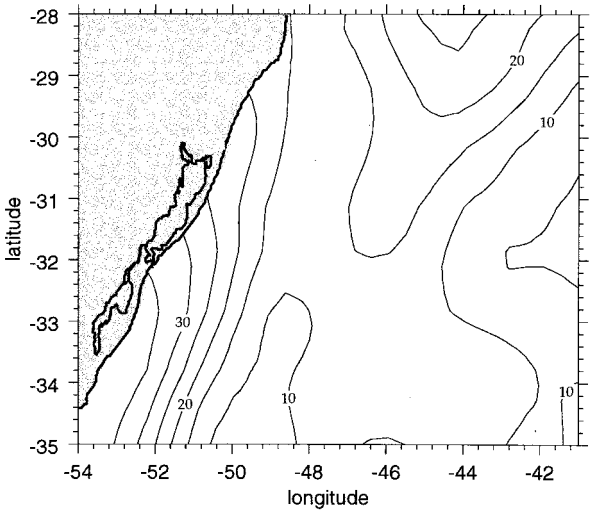

Figure 6. Residual after fitting the observed annual cycle with an idealized sinusoidal curve. The residual is measured as percent relative to the total observed annual range.

annual range generally increases southward, which can be illustrated also by the examples of raw SST series given in Figure 3. As found by *Absy and Zavialov* [1999], the annual cycle of air temperature over the region is similar to that of SST in magnitude, shape, and spatial distribution.

3.2. "Global Change": Secular Trends of SST

After the removal of the seasonal signal the secular SST trend was obtained at all grid nodes by computing the best least squares linear fit to the series of SST anomalies. The spatial distribution of this trend (converted to units of degrees Celsius per 100 years) is shown in Figure 7. Everywhere in the region, the trend is positive, indicating warming. Detailed examination of the SST series (see the examples in Figure 3) reveals that most of this warming has been occurring during the last 6 decades, while little or no trend was observed before the 1940s. It seems also that the increase of winter SSTs was larger than that of summer ones. The analysis performed separately for summer and winter SSTs (not shown) yielded a positive secular trend in both cases. However, at most of the grid nodes the trend in winter series was larger than that in the summer data. On the shelf the area-averaged "winter" trend was nearly twice as large as the "summer" one.

The annual anomalies of SST averaged over the area of the study are shown in Figure 8a for the period 1946 to 1993. For comparison, Figure 8b depicts similar information derived from the Comprehensive Ocean-Atmosphere Data Set (COADS) [e.g., *Woodruff et al*., 1987], available for that period at 1° spatial resolution. The thin lines indicate the sequence of anomalies for individual years, and the bold curves correspond to a series low-pass filtered with a 11-year-wide moving window in order to highlight the variability in decadal and interdecadal frequency bands. The records of raw anomalies derived from COADS and from local data are correlated at about 0.8 ± 0.1 (the 95% confidence limits were computed through the z criterion of Fisher [e.g., *Anderson*, 1958]). We also investigated basic statistics of the differences between the respective 4224 raw annual anomalies derived from the two sets, at all 88 individual grid nodes. The mean difference was essentially zero with a standard deviation of about 0.25°C, and the linear regression of COADS monthly anomalies against the anomalies derived from the synthesized set yielded intercept zero and slope 0.93 ± 0.08 at 95% confidence level. However, the agreement is less satisfactory in terms of the warming trend. Both data sets reflect a similar increase of SST until about 1964. However, while in the anomalies derived from the synthesized set this positive trend persists until the end of the series, in the COADS based series it is not evident beyond the mid-1960s. Although not supported by COADS data, the tendency toward an increase of SST in the 1970s and 1980s seen in our blended set seems to be consistent with other global records; see, for example, the analysis of *White et al*. [1997] based on the Global Ice Sea Surface Temperature (GISST) data set [*Folland and Powell*, 1994]. As is well known, historical observational products differ considerably one from another. In this paper, we restrict our analysis to the synthesized data set described above.

On a global average, the increase of SST over the past century is believed to be about 0.4°C [e.g., *Lau and Weng*, 1995; *White et al*., 1997]. As can be seen in Figure 7, for most of the area of this study the secular warming is significantly above this global average.

3.2.1. Deep ocean. In the deep ocean part of the region the isopleths of secular trend are oriented predominantly along the shore. From a minimum of about 0.5°C/100 years in the southeastern extremity of the region, the trend increases toward the shelf and attains local maximum with the values over 1.2°C/100 years in a broad zone adjacent to the continental slope, probably controlled by the Brazil Current. In this area the secular warming appears to exceed the global average estimates by approximately a factor of 3.

3.2.2. Shelf. The secular trend shows small local minimum near the shelf break and then continues to grow toward the coast. Over the shelf the warming is remarkably strong (1.2 to 1.6°C/100 years) and is distributed again as a tongue-like pattern narrowing northward. In the alongshore direction the trend tends to increase from north to south. The maximum trend is observed in the areas directly adjacent to the Rio de la Plata estuary and Patos-Mirim complex mouth, suggesting that this anomalously strong secular change may be related to the

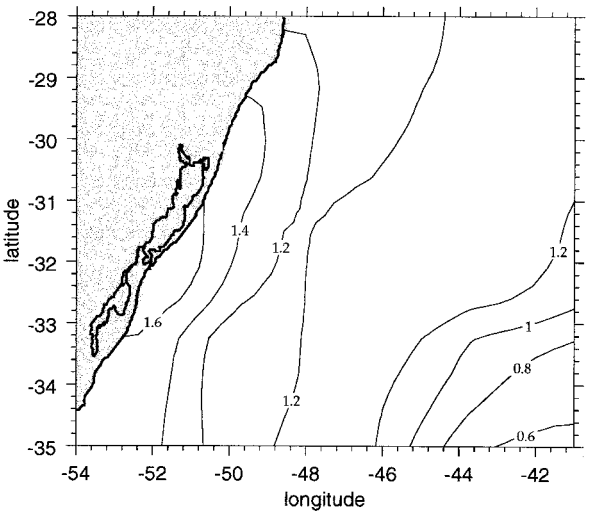

Figure 7. Secular trend of SST, in degrees Celsius per 100 years, found as a slope of best linear fit to the series of monthly SST anomalies.

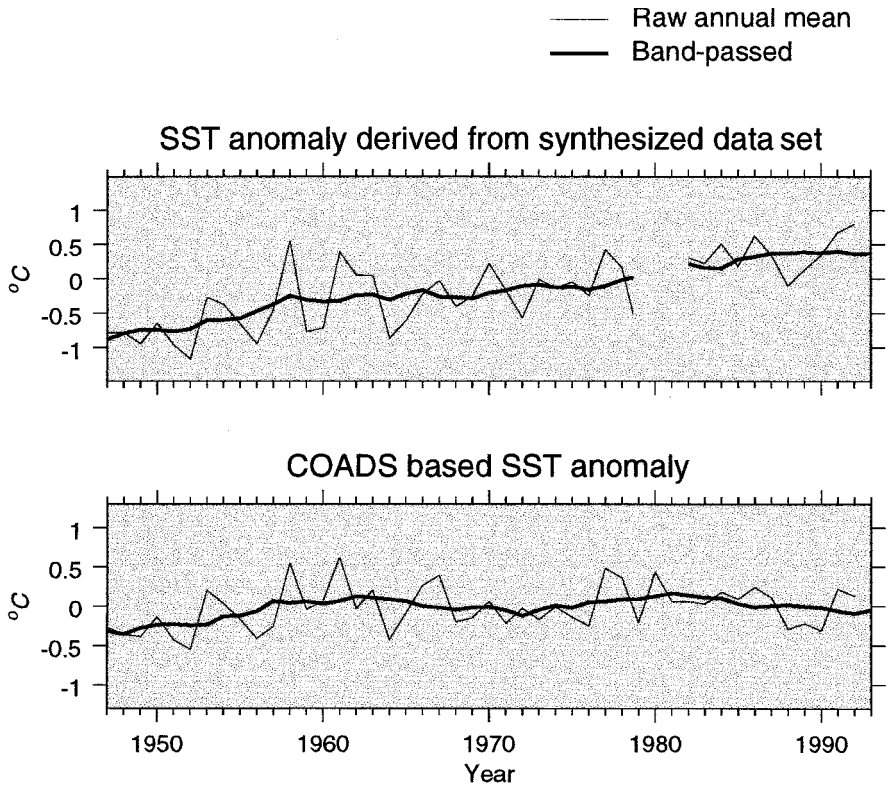

Figure 8. Annual area-averaged SST anomalies (thin lines) derived from the (top) blended data set used in this study and (bottom) the University of Wisconsin-Milwaukee/Comprehensive Ocean-Atmosphere Data Set (UWM/COADS). Bold lines denote same anomalies, but low-pass filtered to highlight decadal and interdecadal variability.

influence of river runoff. The relation between the SST trend in estuarine areas and the variability of hydrological and meteorological conditions in Parana-Paraguay and Patos-Mirim basins is a subject of future research.

3.3. Interannual to Interdecadal Variability: Spatial Pattern and Spectral Content

Next, the secular trends were subtracted from the series of anomalies and the mean square variability was computed. The map in Figure 9 illustrates the spatial distribution of this variability. Overall, it ranges from less than 1°C^2 to over 2.2°C^2.

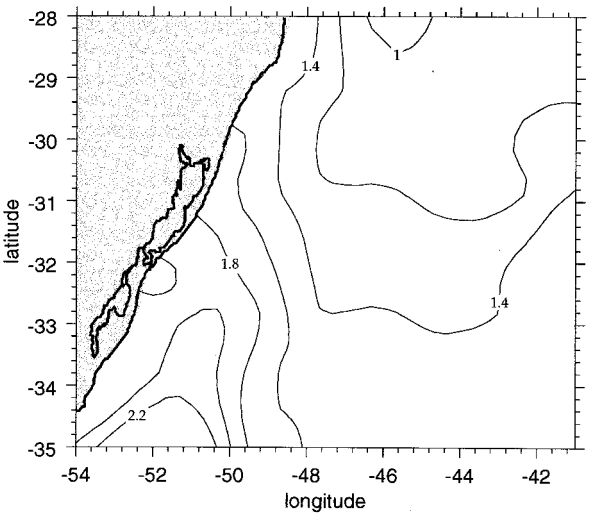

Figure 9. Mean square variability of SST (°C^2), as derived from the series of monthly anomalies.

In order to assess the characteristic temporal scales of the SST variability, we computed the integrated and normalized spectral density functions, which illustrate the partition of the energy of variability into various frequency bands, [e.g., *Weisberg*, 1976]. That is, we computed the function

$$p(t) = \frac{1}{A} \int_{2\pi/t}^{2\pi/t_0} P(\omega)\, d\omega \times 100\% \qquad (2)$$

where $t = 2\pi/\omega$ is period in years, t_0 is some minimum reference period (we used $t_0 = 2$ years), $P(\omega)$ is given by (1), and A is normalizing constant. In this study we took $A = \int_{2\pi/70}^{2\pi/2} P(\omega)\, d\omega$, so that $p(t)$ represents the variability fraction residing at periods between 2 years and t, relative to a total variability at periods between 2 and 70 years. The period of 70 years (a half of the record length) was chosen arbitrarily to serve as a reference.

The integrated spectral density functions were computed at all nodes of the grid (not shown). They generally look alike. In all cases a major part of variability (50 to over 80%) resides at relatively short periods ($t < 10$ yrs). It is interesting, however, to investigate how this relative spectral content depends on spatial coordinates within the region. Figure 10 shows the spatial pattern of the percentage of the variability at periods above 10 years. Here we choose, rather arbitrarily, 10 years as a reference value of the period to distinguish between (relatively) low- and high-frequency bands in variability. With some terminological reservations, it can be said that periods below 10 years characterize interannual variability scale while periods

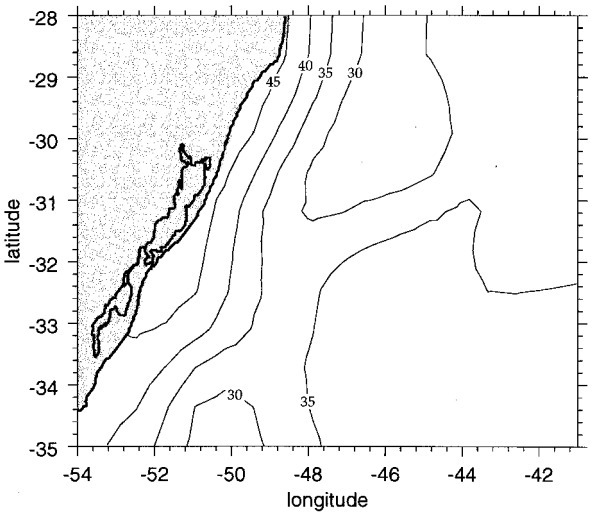

Figure 10. Fraction of SST variability that resides at periods above 10 years, expressed as percent relative to a total variability at periods below 70 years (see text for details).

of 10 years and longer account for decadal and interdecadal scales. In this sense, Figure 10 illustrates the spatial pattern for the relative role of decadal and interdecadal variability. In more formal words, the figure is a map of $100\% - p(10)$, where $p(10)$ is computed as prescribed by (2).

3.3.1. Deep ocean. In most of the deep ocean portion of the region, the overall mean square variability is between 1 and 1.6°C^2 (Figure 9), although higher values can be observed adjacent to the shelf in the south. In the alongshore direction the variability increases from north to south. As almost everywhere in the study area, most of this variability is associated with the interannual scale, while the fraction of variability residing at decadal to interdecadal frequency range is smaller and attains minimum values of less than 30% in two narrow, tongue-like areas near the shelf break (Figure 10).

3.3.2. Shelf. The variability on the shelf is higher than that in the deep part of the study area. Along the coast in the southern part of the region, the already expected tongue-like spatial pattern can be observed, which has been recurrent throughout this study. There the SST variability attains maximum values (up to 2.3°C^2), probably associated with alongshore intrusions of subantarctic waters and, possibly, with variability of freshwater discharges. It can be noted that this position and orientation of the high SST variability zone appear to agree with the field of frontal density computed by *Goni et al*. [1996] through the method of *Garzoli et al*. [1992] and characterizing preferred positions of the frontal zone south of 33°S. They are also in agreement with the area of maximum variability of surface topography as found by *Mata and Garcia* [1996] based on TOPEX/POSEIDON altimeter data.

As can be seen in Figure 10, the relative role of decadal and interdecadal variability is higher over the shelf than in the deep part of the study region and increases toward the coast, where values as high as 40–50% are observed in a narrow belt near the shore.

3.4. Variability of Frontal Position

A pronounced thermohaline front between warm and salty tropical waters and relatively cold and fresh shelf water forms in the study region in austral winter. This part of the discussion will be restricted to the month of July, which was chosen because it had the best historical data coverage of all winter month. As discussed in section 2, we use the 17°C SST isotherm as an indicator of July position of the front. Although it remains to be determined to what degree the position of the isotherm reproduces the "true" position of the frontal zone, there is certainly a close relation between them. For the sake of simplicity, hereafter we refer to the isotherm position as the frontal position.

The data for July were reinterpolated onto a finer, 0.3° × 0.3° grid using the objective analysis scheme of *Levy and Brown* [1986], which uses a variable-size filter of approximately Gaussian shape. Then, a set of maps was plotted (not shown) representing the July positions of the 17°C isotherm for all individual years in order to assess the interannual migrations of the frontal zone. Figure 11 is a summary of this variability. In order to prepare the figure, we first determined the overall mean position of the isotherm, shown as a bold contour labeled "3." All individual years were then grouped in two classes: if in a given year the 17° isotherm merged into the coast north of the mean position, the year was classified as "cold," otherwise it was considered "warm." Figure 11 shows average positions of the isotherm in cold (contour labeled as "2") and warm (contour "4") years. Finally, Figure 11 shows also the northernmost (year 1911, contour "1") and southernmost (year 1992, contour "5") positions observed.

The front-indicative isotherm has a tongue-like shape due to the southward propagation of warm Brazil Current waters along the shelf break. Over the shelf the isotherm is always displaced northward and typically forms an acute angle with the coast. In order to quantify the meridional migrations of the frontal zone, we constructed an index (hereinafter referred to as the front index) of the latitude of its northernmost position, normally the latitude where it merged into the coast. While this simplified parameterization of the frontal position by a single number is by no means adequate to represent the complexity

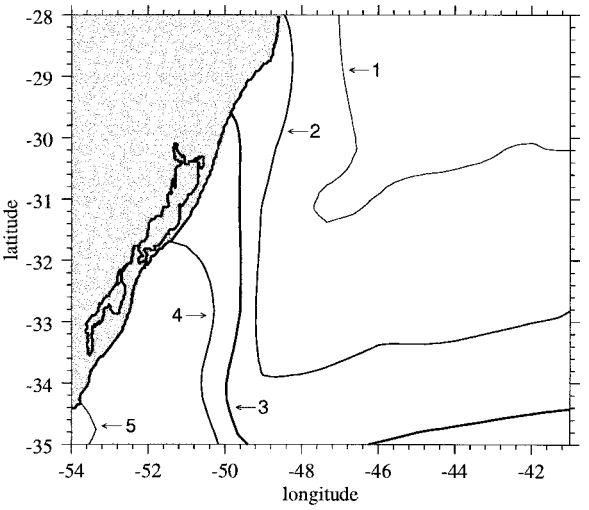

Figure 11. Summary of positions of the frontal zone on the shelf in July. Numbers denote the following: 1, northernmost position observed (1911); 2, average for "cold" years (see text for explanation); 3, overall mean position; 4, average for "warm" years (see text for explanation); and 5, southernmost position observed (1992).

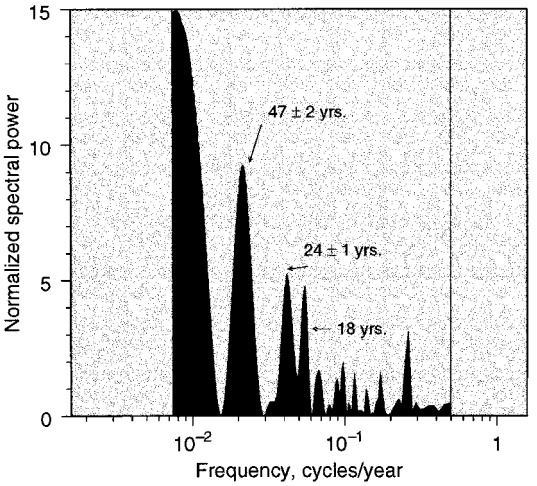

Figure 12. Lomb-Scargle periodogram for the series of northernmost latitude of the frontal zone (front index).

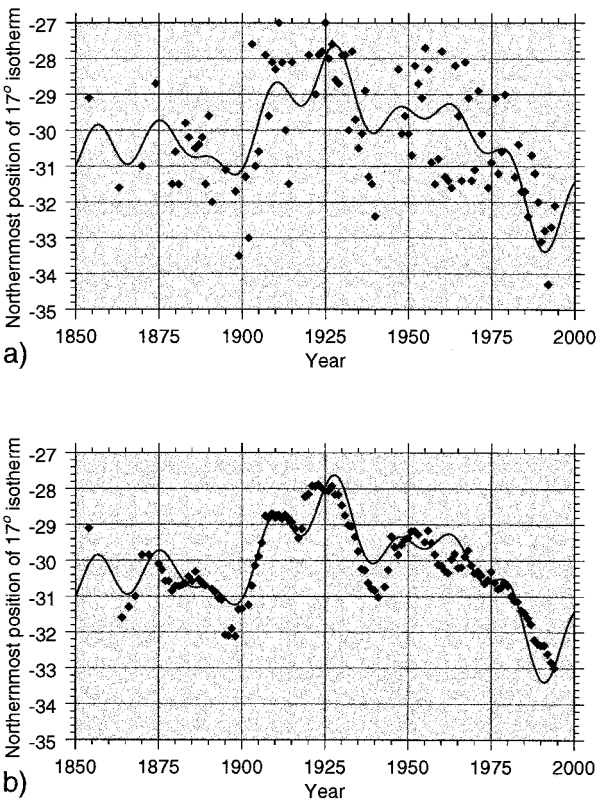

Figure 13. (a) Observed northernmost latitudes of the frontal zone for individual years (diamonds) and a model made up of linear trend and sinusoidal signals corresponding to 18-, 24-, 47-, and 130-year periods (solid curve). (b) Same as Figure 13a, but with observational data low-pass filtered with a 9-year running boxcar filter.

of the dynamics in the region, it can, however, provide a general insight about the migrations of the front along the shore.

The data coverage allowed us to determine the front index for 104 individual years (Figure 13a). In these years the northernmost latitude varied with a range of more than 7° of latitude or about 1400 km of along-coast distance, from about 27.0°S (in 1911) to 34.3°S (in 1992). The mean value was 30.1°S, with a standard deviation of 1.6°. It may be interesting to compare these numbers to the statistics for latitude of separation of the Brazil and Malvinas Currents from the 1000-m isobath reported by *Olson et al*. [1988], although their findings refer to smaller temporal scales. For separations of the Brazil and Malvinas Currents, *Olson et al*. [1988] found mean positions at 35.8°S and 38.8°S, standard deviations of 1.1° and 0.9°, and ranges of 4.8° and 4.4°, respectively.

Best linear fitting to the demeaned series of the front index suggests a southward secular trend at a rate of 0.9° ± 0.2° (or 175 ± 40 km of along-coast distance) per 100 years, significant at 95%. We subtracted this trend from the front index data and then computed the power spectrum of the front index series using Lomb-Scargle periodogram (equation (1)). The periodogram is shown in Figure 12. Significance levels and incertitudes in peak periods were computed through the Lomb-Scargle method as given by *Provost et al*. [1992]. About 50% of the variability is associated with periods below 10 years (note that the abscissa in Figure 12 is logarithmic); however, this high-frequency part of the spectrum is fairly white and has no peaks significant above 50%. At an interdecadal scale there is a major peak at 47 ± 2 years, significant at 99%. There are also two smaller peaks at 24 ± 1 and 18 years, both significant at about 50%. Finally, there is a large increase of spectral power at very low frequencies, with a hint of a broad peak at about 130 years, although the length of data record is, of course, insufficient to ensure it.

As mentioned by *Provost et al*. [1992], the method of Lomb-Scargle periodograms may be subject to spectral leakage; that is, some secondary peaks that appear in the periodogram may actually be "phantoms" of a larger peak. In order to verify whether all peaks are real, the following procedure has been performed. For each of the peak periods we explicitly removed the signal of the corresponding frequency by subtracting it from the data and then computed the spectrum again. If any of the peaks were a product of leakage of the one we had removed, it would vanish after this procedure. All peaks in Figure 12 proved to be real. In addition, we recomputed the spectrum through a conventional FFT procedure after filling out the data gaps with the mean value. This yielded a spectrum (not shown) very similar to that in Figure 12, with the peaks at exactly the same periods.

Furthermore, we constructed a model curve made up of a linear trend and a sum of single-frequency sinusoidal signals corresponding to the spectral peaks revealed from the periodogram. The amplitudes and initial phases of these sinusoidal signals were determined in the following way. First, we subtracted the linear trend from the original front index data. With the detrended series we found the best fitting sinusoidal curve at a frequency of the largest peak and then subtracted this signal from the front index series. With the remainder we found the best fit of a sinusoidal curve at the frequency of the second largest peak, then again subtracted it from the series, and so forth. This procedure was applied to the following peak periods revealed from spectral analysis discussed above: 130, 47, 24, and 18 years.

Even though the length of the data record was insufficient to ensure the peak at 130 years, we included it in the model in order to simulate a contribution from the lowest-frequency component. The sum of linear trend and harmonic signals found thereby determined the model curve. The corresponding analytical expression is

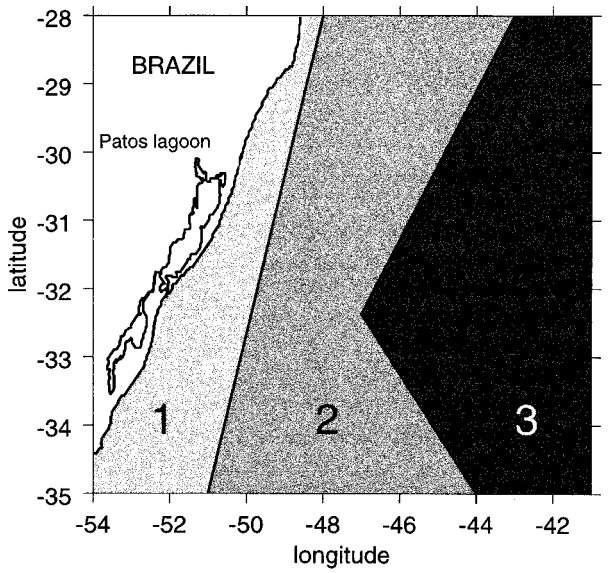

Figure 14. Schematic conceptual representation of the subareas within the region that exhibit distinct behavior with respect to SST variability at annual to secular scales, as discussed in the text.

$$l(t) = -29.25 - (t - 1850) \times 0.009 + 1.3 \cos(2\pi t/130 + 6.24) + 1.0 \cos(2\pi t/47 + 1.67) + 0.7 \cos(2\pi t/24 + 3.77) + 0.5 \cos(2\pi t/18 + 5.43) \quad (3)$$

where l is the northernmost latitude of the front position (front index) and t is time in years.

This model curve is drawn in Figure 13 (solid line). In Figure 13a, diamonds indicate raw data of the front index in individual years. Apparently, there is little agreement between the data and the model curve. This is because of the high-frequency "noise" at interannual scale, which accounts for a considerable part of variability but has no significant isolated peaks and therefore was not included in the model. When this high-frequency component is removed from the data by 9-year low-pass running boxcar filtering, the agreement improves remarkably (Figure 13b).

4. Discussion and Conclusions

As demonstrated, the area of this study is characterized by energetic variability in a range of temporal scales from seasonal to secular. Conceptually, we can divide the region into three areas as schematized in Figure 14, each area exhibiting distinct behavior with respect to the variability at these scales.

1. Area 1 is adjacent to the coast as a belt narrowing northward. The area is over the shelf and appears to be controlled by Rio de la Plata and Patos-Mirim runoff along with invasions of subantarctic water along the coast that occur in austral winter. Consequently, it exhibits an extremely large seasonal cycle of SST (annual range of 7° to more than 10°C), which is also characterized by a large departure from a single annual frequency sinusoidal inference (residual up to 35%). The interannual variations in this area are very energetic as well, with mean square variability ranging from 1.4° to 2.3°C^2. As everywhere in the study region, periods below 10 years account for most of this variability. However, compared with the rest of the region, area 1 is characterized by a relatively large contribution from decadal and interdecadal scales, which at some locations (generally, in the proximity of the estuaries) accounts for up to 50% of variability. The area also shows a very strong secular trend toward warming. The maximum values of up to 1.6°C per 100 years (about 4 times larger than global average) are observed in the proximity of the estuaries. This suggests that anomalous warming may be somehow related to changes in regime of river runoff. The coastal water discharges are likely to have suffered significant changes over the last century owing to agricultural and industrial activities in the river drainages of the Parana-Paraguay basins, which in turn would affect the exposed coastal areas of the ocean. Drastic changes of hydrographic conditions due to human impact have been documented near other large estuaries of the world and in some cases could be traced to a distance of several hundred kilometers from the estuaries [e.g., *Wahby and Bishara*, 1981].

2. Area 2 is in the central part of the region. It may be identified as the area under the influence of the Brazil Current. The seasonal cycle of SST shows fairly high (sometimes up to 30%) residuals from the annual harmonic. However, the range of seasonal variability (5° to 7°C) is moderate compared with that in the shelf. The overall mean square variability ranges from 1° to 1.4°C^2 and is dominated by periods below 10 years. The secular trend is of 1° to 1.2°C per 100 years, i.e., smaller than observed in the area 1, but still high compared with the global average.

3. Area 3 is the eastern deep ocean part of the region. It is away from the influence of either major currents or coastal discharges and therefore, as compared with the rest of the region, exhibits less energetic behavior. This area is characterized by a relatively small (4° to 6°C) and sinusoidal (residuals from annual harmonic are a mere 5 to 15%) seasonal cycle, moderate interannual changes (mean square variability is about 1.2°C^2 in most parts of the area), and a relatively small (0.5° to 1°C per 100 years) secular trend, comparable to the global average.

In winter, owing to the northward flow on the shelf between the Brazil Current and the coast, a thermohaline front forms in the region of this study and in some (although exceptional) years can be traced up to as far north as 27°S. Its northernmost position is subject to strong interannual changes. About half of the energy associated with these excursions resides at periods smaller than 10 years; however, this part of the spectrum is fairly white. In the interdecadal part of the spectrum, at least three individual peaks can be identified (with varying degree of significance), corresponding to periods of 47 ± 2, 27 ± 1, and 18 years. A model curve made up of a linear secular trend (0.9 ± 0.2° of latitude southward per 100 years), sinusoidal signals of these periods, and very low frequency signal corresponding to 130 years showed good agreement with low-passed historical data. An extrapolation of this model curve might even hold promise of prognostic applications. This is, however, certainly beyond the scope of this study. The relationship of the frontal zone variability, associated SST changes, and regional climate impact is a subject of future work.

Acknowledgments. We are grateful to I. S. Kim of Federal University of Pelotas, Brazil, for his contributions to preparation of the

data set used in this paper. Support of Conselho Nacional de Desenvolvimento Científico e Tecnológico of Brazil (CNPq grant 300223/93-5) is gratefully acknowledged by one of the authors (I.W.). I. W. was also supported by Fundação de Amparo a Pesquisa do Estado de Sao Paulo (FAPESP) (grants 98/16346-1 and 93/1387-0). Publication of this study was sponsored by FAPESP. P. Z. was supported by Russian Basic Research Foundation (RBRF) (grant 99-05-65528). We wish to thank two anonymous reviewers for their constructive criticisms and suggestions.

References

Absy, J. M., and P. O. Zavialov, On the variability of air temperature over the southwestern Atlantic ocean, *Atlântica*, in press, 1999.

Anderson, T. W., *An Introduction to Multivariate Statistical Analysis*, 490 pp., John Wiley, New York, 1958.

Bakun, A., and R. H. Parrish, Comparative studies of coastal pelagic fish reproductive habitats: The Brazilian sardine (*Sardinella aurita*), *J. Cons. Cons. Int. Explor. Mer.*, *46*, 269–283, 1990.

Bakun, A., and R. H. Parrish, Comparative studies of coastal pelagic fish reproductive habitats: The anchovy (*Engraulis anchoita*) of the southwestern Atlantic, *J. Mar. Sci.*, *48*, 343–361, 1991.

Chelton, D. B., M. G. Schlax, D. L. Witter, and J. G. Richman, Geosat altimeter observations of the surface circulation of the southern ocean, *J. Geophys. Res.*, *95*, 17,877–17,903, 1990.

Cheney, R. E., J. G. Marsh, and B. D. Beckley, Global mesoscale variability from collinear tracks of Seasat altimetry data, *J. Geophys. Res.*, *88*, 4343–4351, 1983.

Ciotti, A. M., C. Odebrecht, G. Fillmann, and O. O. Moller Jr., Freshwater outflow and Subtropical Convergence influence on phytoplankton biomass on the southern Brazilian continental shelf, *Cont. Shelf Res.*, *15*, 1737–1756, 1995.

Confluence Principal Investigators, Confluence 1988–1990: An intensive study of the southwestern Atlantic, *Eos Trans. AGU*, *71*, 1131–1133, 1137, 1990.

Folland, D. K., and D. P. Powell, The standard GISST data sets: Version 1 and 2, *Clim. Res. Tech. Note 56*, pp. 50–51, Hadley Cent. for Clim. Predict. and Res., Meteorolol. Off., Bracknell, England, 1994.

Garzoli, S. L., Geostrophic velocity and transport variability in the Brazil-Malvinas Confluence, *Deep Sea Res., Part I*, *40*(7), 1379–1403, 1993.

Garzoli, S. L., and Z. Garraffo, Transports, frontal motions and eddies at the Brazil-Malvinas Currents Confluence, *Deep Sea Res., Part A*, *36*, 681–703, 1989.

Garzoli, S. L., and C. Giulivi, What forces the variability of the southwestern Atlantic boundary currents?, *Deep Sea Res., Part I*, *41*, 1527–1550, 1994.

Garzoli, S. L., and C. Simonato, Baroclinic instabilities and forced oscillations in the Brazil/Malvinas confluence front, *Deep Sea Res., Part A*, *37*, 1053–1074, 1990.

Garzoli, S. L., Z. Garraffo, G. Podesta, and O. Brown, Analyses of a general circulation model product, 1, Frontal systems in the Brazil/Malvinas and Kuroshio/Oyashio regions, *J. Geophys. Res.*, *97*, 20,117–20,138, 1992.

Goni, G., S. Kamholz, S. Garzoli, and D. Olson, Dynamics of the Brazil-Malvinas confluence based on inverted echo sounders and altimetry, *J. Geophys. Res.*, *101*, 16,273–16,289, 1996.

Gordon, A. L., South Atlantic thermocline ventilation, *Deep Sea Res., Part A*, *28*, 1239–1264, 1981.

Gordon, A. L., Brazil-Malvinas Confluence—1984, *Deep Sea Res., Part A*, *36*, 359–384, 1989.

Gordon, A. L., and C. L. Greengrove, Geostrophic circulation of the Brazil-Falkland confluence, *Deep Sea Res., Part A*, *33*, 573–585, 1986.

Guerrero, R. A., E. M. Acha, M. B. Framiñan, and C. A. Lasta, Physical oceanography of Rio de la Plata estuary, Argentina, *Cont. Shelf Res.*, *17*, 727–742, 1997.

Horne, J. H., and S. L. Baliunas, A prescription for analysis of unevenly spaced sampled time series, *Astrophys. J.*, *263*, 835–853, 1986.

Hubold, G., Hydrography and plankton off Southern Brazil and Rio de la Plata (August–November 1977), *Atlântica*, *4*, 1–78, 1980.

Kim, I. S., and P. O. Zavialov, Relação entre variações da temperatura do mar e características do clima na região sul do Brasil, in *Proceedings of VII Congresso Latinoamericano e Ibérico de Meteorología*, pp. 355–356, Fed. Latinoamericana e Ibérica de Meteorol., Buenos Aires, Argentina, 1996.

Lau, K. M., and H. Weng, Climate signal detection using wavelet transform: How to make a time series sing, *Bull. Am. Meteorol. Soc.*, *76*, 2391–2402, 1995.

Legeckis, R. V., and A. L. Gordon, Satellite observations of the Brazil and Falkland currents–1974 to 1976 and 1978, *Deep Sea Res., Part A*, *29*, 375–401, 1982.

Levy, G., and R. A. Brown, A simple objective analysis scheme for scatterometer data, *J. Geophys. Res.*, *91*, 5153–5158, 1986.

Lima, I. D., and J. P. Castello, Distribution and abundance of Southwest Atlantic anchovy spawners (Engraulis anchoita) in relation to oceanographic processes in the southern Brazilian shelf, *Fish. Oceanogr.*, *4*(1), 1–16, 1995.

Lima, I. D., C. A. E. Garcia, and O. O. Moller Jr., Ocean surface processes in the Southern Brazilian shelf: Characterization and seasonal variability, *Cont. Shelf Res.*, *16*(10), 1307–1317, 1996.

Lomb, N. R., Least squares frequency analysis of unequally spaced data, *Astrophys. Space Sci.*, *39*, 447–462, 1976.

Maamaatuaiahutapu, K., V. C. Garçon, C. Provost, M. Boulahdid, and A. P. Osiroff, Brazil-Malvinas confluence: Water mass composition, *J. Geophys. Res.*, *97*, 9493–9506, 1992.

Mata, M. M., and C. A. E. Garcia, Variabilidade da topografia oceânica no Atlântico Sul Ocidental observada pela altimetria TOPEX/POSEIDON, *Proceedings VIII Simposio Brasileiro do Sensoriamento Remoto* (CD-ROM), Inst. de Pesqui. Espaciais, Sao Paulo, 1996.

Matano, R. P., On the separation of the Brazil Current from the coast, *J. Phys. Oceanogr.*, *23*, 79–90, 1993.

Matano, R. P., M. G. Schlax, and D. B. Chelton, Seasonal variability in the southwestern Atlantic, *J. Geophys. Res.*, *98*, 18,027–18,035, 1993.

Olson, D. B., G. P. Podesta, R. H. Evans, and O. B. Brown, Temporal variations in the separation of Brazil and Malvinas Currents, *Deep Sea Res., Part A*, *35*, 1971–1990, 1988.

Peterson, R. G., and L. Stramma, Upper-level circulation in the South Atlantic ocean, *Prog. Oceanogr.*, *26*, 1–73, 1991.

Podesta, G. P., Migratory pattern of Argentina hake merluccius hubbsi and oceanic processes in the Southern Atlantic Ocean, *Fish. Bull.*, *88*, 167–177, 1990.

Provost, C., O. Garcia, and V. Garçon, Analysis of sea surface temperature time series in the Brazil-Malvinas currents confluence region: Dominance of the annual and semiannual periods, *J. Geophys. Res.*, *97*, 17,841–17,858, 1992.

Provost, C., V. Garçon, and L. M. Falcon, Hydrographic conditions in the surface layers over the slope—Open ocean transition area near the Brazil-Malvinas Confluence during austral summer 1990, *Cont. Shelf Res.*, *16*(2), 215–235, 1996.

Reid, J. L., On the total geostrophic circulation of the South Atlantic Ocean: Flow patterns, tracers and transports, *Prog. Oceanogr.*, *23*, 149–244, 1989.

Reynolds, R. W., A real-time global sea surface temperature analysis, *J. Clim.*, *1*, 75–86, 1988.

Reynolds, R. W., and D. C. Marsico, An improved real-time global sea surface temperature analysis, *J. Clim.*, *6*, 114–119, 1993.

Reynolds, R. W., and T. M. Smith, Improved global sea surface analyses using optimum interpolation, *J. Clim.*, *7*, 929–948, 1994.

Reynolds, R. W., C. K. Folland, and D. E. Parker, Biases in satellite derived sea-surface-temperatures, *Nature*, *341*, 728–731, 1989.

Roden, G. I., Thermohaline fronts and baroclinic flow in the Argentine Basin during the austral spring of 1984, *J. Geophys. Res.*, *91*, 5075–5093, 1986.

Scargle, J. D., Studies in astronomical time series analysis, II, Statistical aspects of spectral analysis of unevenly spaced data, *Astrophys. J.*, *263*, 835–853, 1982.

Wahby, S. D., and N. F. Bishara, The effect of the river Nile on Mediterranean water, before and after the construction of the High Dam at Aswan, in *River Inputs to Ocean Systems*, edited by J.-M. Martin, J. D. Burton, and D. Eisma, pp. 311–315, UNESCO, Paris, 1981.

Weisberg, R. H., The nontidal flow in the Providence river of Narragansett Bay: A stochastic approach to estuarine circulation, *J. Phys. Oceanogr.*, *6*, 721–734, 1976.

White, W. B., D. R. Cayan, and M. D. Dettinger, Response of global upper ocean temperature to changing solar irradiance, *J. Geophys. Res.*, *102*, 3255–3266, 1997.

Woodruff, S. D., R. J. Slutz, R. L. Jenne, and P. M. Steurer, A comprehensive ocean-atmosphere data set, *Bull. Am. Meteorol. Soc.*, *68*, 1239–1250, 1987.

Zavialov, P. O., and J. M. Absy, Variabilidade interdecadal e inter-

anual na região da Confluência Brasil–Malvinas revelada através de dados historicos desde 1854, in *Proceedings of IX Semana Nacional de Oceanografia*, pp. 511–513, Itajaí, Brazil, 1997.

Zavialov, P. O., and I. S. Kim, A study on marine climatology in the South Brazilian coastal waters, in *Proceedings of VII Congresso Latinoamericano e Ibérico de Meteorología*, pp. 277–278, Fed. Latinoamericana e Ibérica de Meteorol., Buenos Aires, Argentina, 1996.

Zavialov, P. O., R. D. Ghisolfi, and C. A. E. Garcia, An inverse model for seasonal circulation over the Southern Brazilian shelf: Near-surface velocity from the heat budget, *J. Phys. Oceanogr.*, *28*, 545–561, 1998.

J. M. Absy, Department of Physics, University of Rio Grande, CP 474, Rio Grande, RS 9620-900 Brazil.

I. Wainer, Oceanographic Institute, University of São Paulo, Praca do Oceanografico 191, 05508-900, São Paulo, Brazil.

P. O. Zavialov, Laboratory of Experimental Physics of the Ocean, P. P. Shirshov Institute of Oceanology, Nakhimovsky Prospekt 36, Moscow 117851, Russia (peter@lpi.ru).

(Received March 6, 1998; revised September 23, 1998; accepted November 17, 1998.)